DNA-Based Nanoprobes for Fluorescence K+ Sensing in Neural Systems

Bryce Dunn,†[a] Madinah Azizi,*[b] Sally Farag,*[a] Laura McAuliffe,[c] John R. Cressman,[d,e] Remi Veneziano,[a,e] Parag V. Chitnis[a,e]

[a]George Mason University, Department of Bioengineering, Fairfax, USA
[b]George Mason University, Department of Systems Biology, Fairfax, USA
[c]George Mason University, Department of Psychology, Fairfax, USA
[d]George Mason University, Department of Physics and Astronomy, Fairfax, USA
[e]George Mason University, Center for MedTech Innovation, Fairfax, USA
*These authors contributed equally to this work

Abstract

Significance: Abnormalities in potassium ion concentrations across subregions of the hippocampus have been implicated in seizures and other pathologies. Direct measurements of potassium ion concentrations are largely made using invasive electrodes, which do not allow for wide spatial coverage. This fluorescent nanoparticle potassium sensor enables direct visualization of potassium dynamics and represents a minimally invasive alternative to electrode-based methods.

Aim: Here, we present a DNA-based fluorescence nanoprobe capable of sensing relative concentrations of potassium ions within populations of neurons. We present its effectiveness in monitoring neuronal K^+ dynamics in response to electrical stimulation ex vivo.

Approach: We used widefield fluorescence microscopy to monitor changes in fluorescence intensity in labeled brain tissue in response to electrical stimulation ex vivo.

Results: We found that our nanoprobe could be retained within the intracellular compartment and modulate in fluorescence intensity linearly in response to induced electrical current. Our K^+ Sensor showed a fractional fluorescence change of approximately 1% per 10 mA of applied stimulation current in brain tissue. Optical spectroscopy confirmed the selectivity of the nanoprobes to potassium ions over other endogenous ions.

Conclusions: Our findings indicate that this nanoprobe can be used to detect more complex potassium dynamics implicated in various pathologies of the nervous system, such as migraines, seizures, and trauma.

Keywords: DNA-based probe, aptamer, nanoprobes, fluorescence, hippocampus, potassium.

† First Author, E-mail: bdunn6@gmu.edu
Correspondence should be addressed to rvenezia@gmu.edu and pchitnis@gmu.edu

1 Introduction

Potassium is the most abundant intracellular cation that contributes to many physiological processes. In neurons, potassium (K^+) plays a crucial role in signal transmission by maintaining the resting membrane potential, shaping action potential generation, and contributing to the refractory period through membrane hyperpolarization [1], [2], [3], [4]. The neuronal membrane potential closely reflects the potassium equilibrium potential, which is largely determined by the

ratio of intracellular to extracellular K^+ concentrations. Potassium is maintained at a 30–40-fold higher concentration inside cells (~150 mM) than in the extracellular space (3.5–5.0 mM), contributing to a resting membrane potential of approximately −70 to −80 mV [5], [6], [7], [8]. During action potentials, neurons release K^+ into the extracellular space during the repolarization phase, leading to transient increases in extracellular K^+ concentration [9]. Activation of K^+ channels promotes membrane hyperpolarization, stabilizing the membrane potential, and suppressing excessive excitatory signaling in neurons [10]. Disruption of K^+ homeostasis alters neuronal excitability and synaptic transmission, and is associated with neurological disorders including epilepsy, Parkinson's disease, autism spectrum disorder, and Alzheimer's disease [11], [12], [13], [14], [15], [16]. Thus, elucidating K^+ ion flux dynamics is essential for understanding pathological mechanisms driving these conditions.

Several approaches have been developed to monitor potassium dynamics *in vitro* and *in vivo*. Ion-selective electrodes have been a gold standard method for quantitative measurements of absolute potassium concentration [3], [17], [18], [19], [20]. While offering good temporal resolution, they are invasive and lack wide spatial coverage, constraining their use for monitoring spatiotemporal dynamics of K^+ flux. Fluorescent indicators offer a complementary approach, enabling wide-field spatial coverage with high temporal resolution but without the tissue disruption associated with electrode placement. Most available fluorescent K^+ sensors have been developed for extracellular measurements, with only a limited number designed for intracellular imaging [21], [22], [23], [24].

We have developed a fluorescent DNA nanoparticle-based sensor designed for the detection of potassium ions in biological environments. Our nanoprobe leverages a K^+ aptamer, functionalized with a rhodamine derivative, ATTO Rho101 (ATTO-TEC, Ex. 587 nm, Em. 609

nm), and a quencher dye, IowaBlack (Integrated DNA Technologies, peak absorbance: 656 nm) with overlapping emission and absorbance spectra, respectively (Fig. 1a). Upon interacting with potassium ions, a conformational change in the DNA nanostructure results in G-quadruplex formation (Fig. 1b). The formation of the G-quadruplex brings the fluorophore and the quencher in close proximity, producing a FRET-based quenching effect [25], [26]. This real-time fluorescence quenching provides an optical measure of potassium ion concentration changes within the cellular milieu.

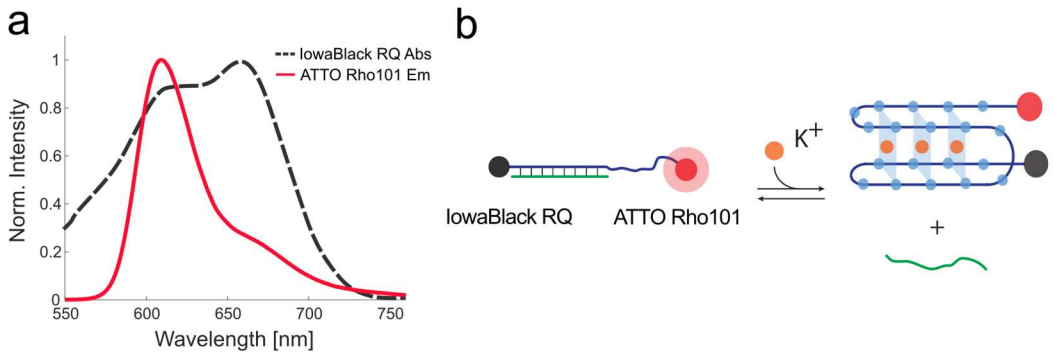

Fig. 1 Optical components and molecular design of the DNA-aptamer potassium sensor. (a) Relative absorbance spectra of IowaBlack and relative emission spectra of ATTO Rho101. (b) Schematic of molecular design of the potassium sensor and FRET quenching during G-quadruplex formation.

In this study, we observed fluorescence intensity responses to intracellular potassium ion dynamics following electrical stimulation of the labeled mouse hippocampus. Timelapse imaging was performed to quantify changes in fluorescence intensity within the hippocampal neurons in response to induced electrical stimulation trains. Spectral measurements helped confirm selectivity and fluorescence response. These results are promising because intracellular K+ imaging is inherently challenging because the high resting potassium concentration (~150 mM) necessitates sensing elements that must discriminate K^+ from competing ions such as Na^+. Our probe fills an unmet need for an intracellular, FRET-quenching fluorescent sensor for applications in neural tissue.

2 Materials and Methods

2.1 Synthesis of the K^+ Sensor

The two DNA oligonucleotides strands (modified and non-modified) were purchased from Integrated DNA Technologies (IDT) in dried form, resuspended in water without further purification, and stored at -20ºC prior to being used. The sequences are listed in Supplementary Table S1. The K^+ aptamer sensor strand is a 27 bases long single strand labeled in its 5'-end with an ATTO Rho101 dye and with Iowa Black RQ quencher at its 3'-end (Table S1). The K^+ Sensor additionally includes a complementary blocker strand of 18 bases, which maintains the spatial separation of the dye and quencher by creating a duplex in the absence of potassium. The sensor was folded by combining both strands at an equimolar concentration of 10 µM in a TAE Folding Buffer (40 mM Tris, 20 mM acetic acid, 2 mM ethylenediaminetetraacetic acid [EDTA], and complemented with 12 mM magnesium chloride [$MgCl_2$] at pH 8.0) with slow annealing over 2 hours from 90°C to 4°C in a Biorad T100 thermocycler. The sensor was then stored at 4°C until further use. The duplex formation was confirmed with polyacrylamide gel electrophoresis (PAGE), using a 20% gel in Tris acetate EDTA (TAE) buffer. 10 µL of samples at 5 µM were loaded with 1X Gel Loading Dye Purple (B7025S; New England BioLabs) and ran for 2 hours at 100 V. The gel was then stained for 10 minutes in a SYBR Safe (S33102; Thermo Fisher Scientific) solution and imaged with Azure c150 blue transilluminator.

2.2 Spectral Characterization of K^+ Sensor

Measurements of fluorescence emission were carried out using a StarLine spectrometer (Avantes) and HAL-Mini halogen lamp (Avantes) and measured using AvaSoft (Version 8). Measurements were made in quartz cuvettes (ThorLabs) using 100 µL samples. Emission response to potassium

106 ions was conducted in K^+ Sensor diluted in milliQ water. Emission spectra were measured in a
107 range from 500-700 nm using broadband excitation. Investigations of metal cation effect in the
108 concentration range of 0-20 mM consisted of serial dilutions of a concentrated solution of 1 M
109 KCl, 1 M NaCl, 1 M $MgCl_2$, or 1 M $CaCl_2$ (Sigma Aldrich), followed by stirring. Studies of the
110 metal cation effect were carried out at 25°C.

111 *2.3 Cellular Imaging*

112 HeLa cells were cultured on an uncoated #1.5 glass coverslip in media for 24 hours. Samples were
113 labeled with FITC at 500 nM, Hoechst 33342 (NucBlue), and K^+ Sensor at 500 nM. Microscopy
114 imaging experiments were performed with a Zeiss LSM800 inverted microscope stand. FITC
115 channel acquired 493 nm excitation and 400–575 nm emission detection at 2.0 Airy units. K^+
116 Sensor channel acquired with 587 nm excitation and 565–700 nm emission detection at 2.5 Airy
117 units. Hoechst channel was acquired with 348 nm excitation and 400–600 nm emission detection
118 at 2.0 Airy units. The laser scan pixel time for every channel is 1.469E-06 sec. Confocal
119 fluorescence images were taken using a 63×/1.4 Plan Apochromat oil immersion objective. Voxel
120 size: 0.0706×0.0706×0.37 μm^3 with 16 bits per pixel.

121 *2.4 Animal Tissue Imaging*

122 Acute hippocampal slices (400 µm-thick) were prepared from Adult C57BL6/J mice (male and
123 female, P30-90) using a tissue chopper. Slices were incubated at room temperature for one hour in
124 prepared artificial cerebrospinal fluid (126 mM NaCl, 3 mM KCl, 2 mM $CaCl_2$, 2 mM $MgCl_2$, 2
125 mM NaH_2PO_4, 26 mM $NaHCO_3$, 10 mM D-Glucose), aerated with carbogen, prior to labeling. For
126 fixed imaging, brain slices were stained with 500 nM of K^+ Sensor and mounted between a glass
127 slide and a #1.5 glass coverslip with a plastic spacer using ProLong mounting medium. Imaging

128 was performed using a Zeiss LSM800 inverted microscope stand. Widefield fluorescence image
129 was taken using a 10×/0.25 NA Achroplan air objective and Axiocam 820 camera. K^+ Sensor
130 channel acquired with 587 nm excitation and 565–700 nm emission detection. Image size:
131 1227.52×1236.288 μm (1120×1128 pixels).

132 Live recordings of brain slices were performed as follows: brain slices were stained with
133 500 nM of K^+ Sensor and mounted in a custom recording chamber for immersion imaging in
134 prepared artificial cerebrospinal fluid perfused with carbogen (Roberts Oxygen, 95% O_2, 5% CO_2).
135 Images were acquired on a BX51WI Upright Microscope (Olympus) custom-modified with a
136 translational stage, configured for widefield epifluorescence microscopy and controlled with
137 Micro-Manager (MMStudio Version 2.0.0), equipped with a 10×/0.3 LUMPlanFL water
138 immersion objective (Olympus). Images had a width and height of 3200 pixels, 1 plane (z), and 1
139 channel. K^+ sensor was excited with a LS200US Metal Halide light source (Lumen) set to 100%;
140 wavelength selection was carried out using a FEBP532-30 bandpass filter (ThorLabs),
141 DMLP605R dichroic mirror (ThorLabs), and a longpass emission filter FELH0600 (ThorLabs).
142 Images were acquired on a Kinetix sCMOS camera (Teledyne) with an exposure time of 50 ms
143 with 1×1 binning.

144 Electrical stimulation pulses were delivered using a Model 2100 Isolated Pulse Stimulator (A-
145 M Systems). Voltage measurements were made using a Digidata 1440 Series digitizer (Molecular
146 Devices) and Clampex software (Version 10).

147 *2.5 MTT Assay for Cell Viability*

148 The MTT assay for cell viability (Roche) was performed using a microplate reader (Thermo
149 Fisher) running SkanIt (Version 7.0). HeLa cells were cultured and seeded into a 96-well plate at
150 5000 cells per well and incubated at 37°C for 24 hours. Cells were expected to reach approximately

151 10,000 per well at the time of treatment, based on standard doubling time. Treatment groups (n =
152 5) were administered dimethyl sulfoxide, and concentrations of K+ Sensor (250 nM, 500 nM and
153 1000 nM) directly into the well plate before adding 10 µL of MTT. The well plate incubated
154 overnight as the MTT was converted to formazan. After this incubation period, the formazan was
155 dissolved using a solubilization buffer containing sodium dodecyl sulfate (SDS). Optical
156 absorbance was read at 570 nm. Wells filled with molecular biology grade water were used as
157 blanks. Results (Fig. S2) were normalized to cells that were not incubated with the K^+ Sensor or
158 DMSO. DMSO was used as a separate, negative control.

159 **3 Results**

160 *3.1 Synthesis and characterization of the K^+ Sensor*

161 To monitor K^+, we designed an aptamer-based sensor (K^+ aptasensor) using a modified version of
162 the design proposed by Yang et al. [27]. Here we used the K^+ aptamer strand labeled with ATTO
163 Rho101 and IowaBlack RQ at its 5'- and 3'- ends, respectively and hybridized it with a
164 complementary blocker strand (Figure 1b and table S1). The blocker strand creates a duplex to
165 maintain the spatial separation of the fluorophore and the quencher in the absence of potassium
166 ions. To validate the assembly of the duplex, we ran a 20% PAGE gel with 10 µL of each strand
167 along with the duplex at 5 µM concentration seen in Figure S1. The results show a clear formation
168 of the duplex with increased molecular weight and no byproduct as expected for this type of
169 construct.

170 *3.2 Spectral Characterization of K^+ Sensor*

171 We performed optical characterization to demonstrate two key design points: emission quenching
172 in response to potassium ions, and selectivity of the sensor to endogenous metal ions as measured

173 by fluorescence emission intensity. The response of the nanoprobe (100 nM in deionized water) to
174 increasing potassium ion concentration, shown in Fig. 2a, demonstrates emission intensity
175 decrease. This emission quenching is further characterized in Fig. 2b by showing a linear
176 relationship between intensity at the peak emission wavelength (610 nm, Fig. 2b cutaway plot)
177 and potassium ion concentration, which is conserved for varying concentrations of K^+ Sensor.
178 Fig. 2c demonstrates the selectivity of the K^+ Sensor when tested against common endogenous
179 metal ions. It is known that there are approximately 100 mM potassium ions in living cells, and
180 when undergoing depolarization, the concentration may shift by approximately 10 mM [28], [29].
181 Together, these results indicate a potassium-selective, fluorescence emission intensity quenching
182 response in physiologically relevant ion concentrations.

183 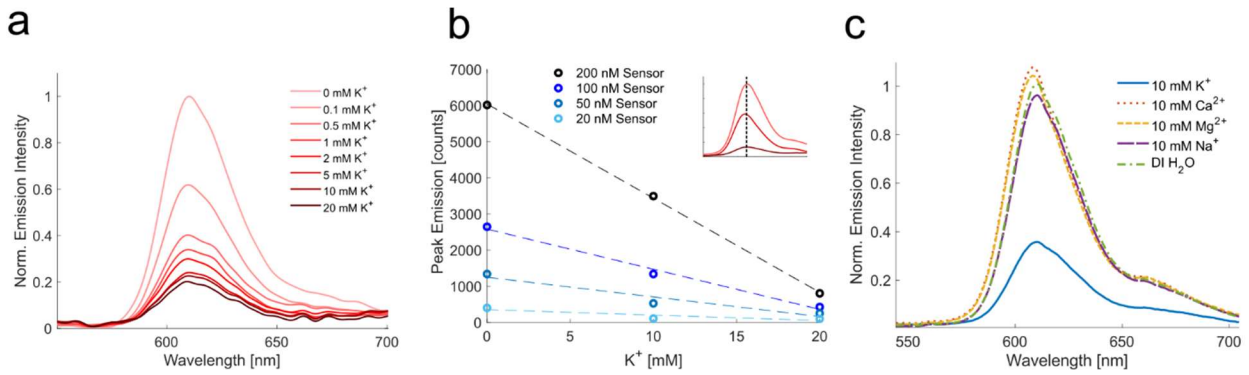

184 **Fig. 2** Optical properties of the DNA-aptamer potassium sensor in solution. (a) Relative emission
185 intensity of 100 nM potassium sensor in 0, 0.1, 0.5, 1, 2, 5, 10, and 20 mM potassium chloride
186 solution. (b) Peak emission intensity at 610 nm wavelength (cutaway) by potassium concentration
187 for varying concentrations of potassium sensor. (c) Relative emission intensity of 100 nM
188 potassium sensor in 10 mM potassium chloride, 10 mM calcium chloride, 10 mM magnesium
189 chloride, 10 mM sodium chloride, and deionized water.

190 *3.3 Cellular Imaging*

191 We performed labeling and imaging experiments to show the spatial distribution of the K^+ sensor
192 in cell and tissue models. A HeLa model labeled with FITC, K^+ Sensor, and Hoechst (Fig. 3a)
193 demonstrates that the K^+ Sensor enters the intracellular space between the plasma membrane and

194 nuclear membrane. Labeling an acute brain slice with K^+ Sensor shows cellular uptake of the
195 nanoprobe into the bodies of hippocampal neurons (Fig. 3b). Additionally, the application of K^+
196 Sensor in a HeLa model does not significantly impact cell viability or metabolic activity compared
197 to untreated cells (0 mM K^+ Sensor), as measured via MTT assay (Fig. S2).

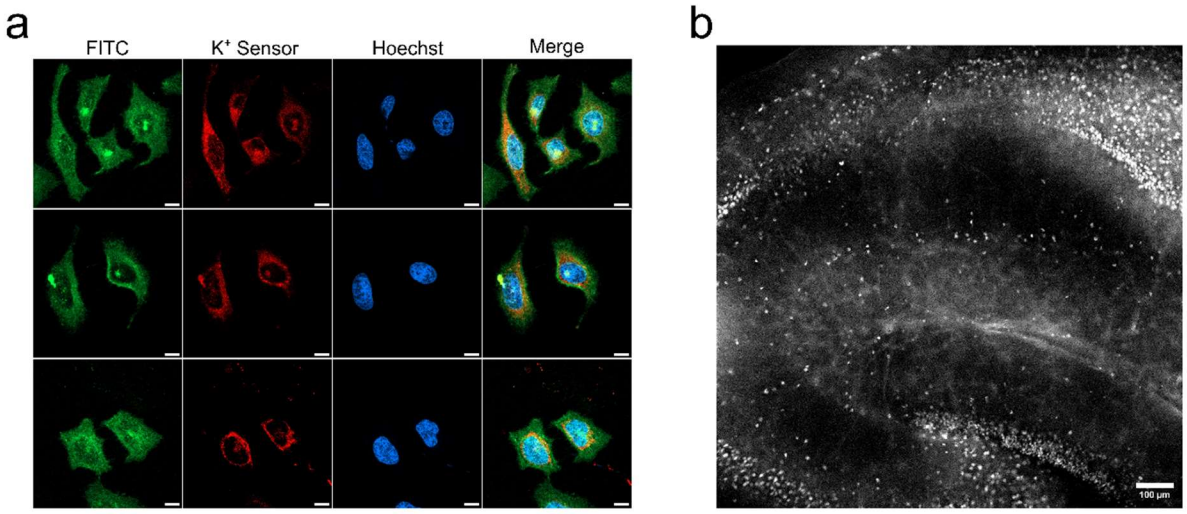

198

199 **Fig. 3** K^+ sensor labeling of cell and tissue models. (a) Confocal fluorescence microscopy images
200 of HeLa cells labeled with FITC (green), K^+ Sensor (red), and Hoechst (blue). Confocal images
201 are presented as maximum intensity projections. Scale bar: 10 µm. (b) Widefield fluorescence
202 image of acute hippocampus slice labeled with K^+ sensor. Scale bar: 100 µm.

203 Confocal microscopy images confirm that the nanoprobe is internalized within the cell, where
204 it interacts with intracellular potassium ions. Several studies have produced extracellular
205 nanoparticle potassium sensors, and few have produced intracellular sensors [24], [27]. A study
206 by Müller et al. produced a BODIPY-based intracellular potassium ion sensor for neural
207 applications [30]. Their results suggest that energy-dependent endocytosis is the primary
208 mechanism of cell entry. We observed efficient labeling of acute brain slice tissue in thirty minutes,
209 in contrast to three-hour staining observed in the study by the Müller group.

3.4 Electrical Stimulation of Murine Brain Tissue

After confirming intracellular K^+ sensor labeling, we demonstrated fluorescence intensity changes in tissue following pulsed electrical stimulation in labeled mouse brain tissue. The aim of this experiment is to visualize electrical stimulation of the canonical Schaffer Collateral [31], [32], stimulating the tissue in the CA3 region of the hippocampus and recording fluorescence response in the CA1 region (Fig. 4a). Using electrical stimulation paradigms of 2.5, 20, 30, and 40 mA, corresponding fluorescence intensity responses are observed (Fig. 4b). Stimulation currents in the milliampere range were required to produce detectable population-level fluorescence responses, likely due to current losses at the extracellular electrode-tissue interface and the requirement for synchronous recruitment of labeled neurons to generate a measurable optical signal. Responses were not observed at microampere-range currents. Neuronal cell bodies labeled with K^+ Sensor demonstrate fluorescence intensity changes of approximately 0.5% in response to 2.5 mA stimulation current (Fig. S3) where a recording electrode in the extracellular space shows a 12-mV potential change. Fluorescence response to higher, 40 mA electrical stimulations can be visualized proximally to the stimulating electrode (Fig. S4). There is variation between sensor responses depending on several factors such as the precise positioning of the stimulating electrode within the CA3, positioning of the recording electrode in CA1, and positioning of the region of interest for analysis.

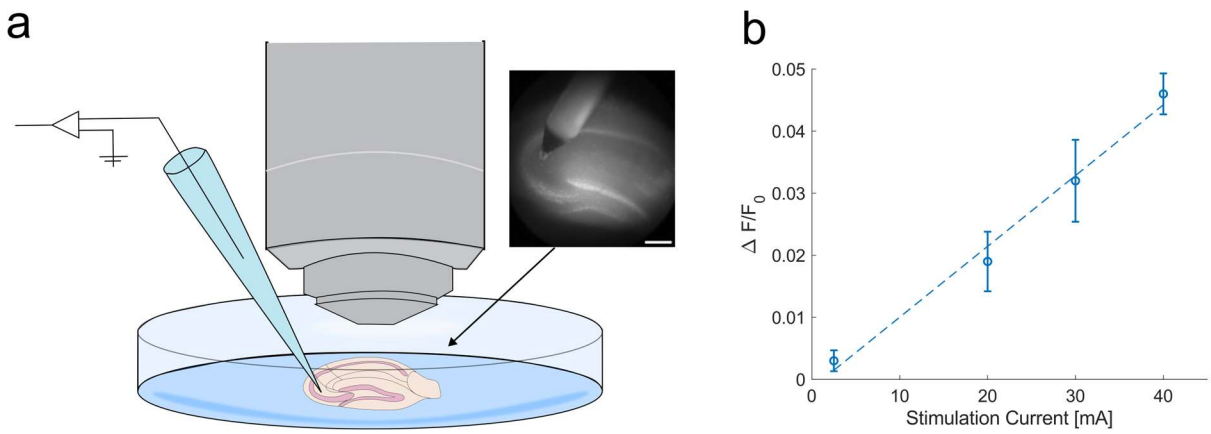

Fig. 4 Electrical stimulation of labeled acute brain slices. (a) Schematic representation of sample and electrode placement in the recording chamber. Cutaway is a widefield fluorescence image of the labeled hippocampus with the stimulating electrode. Scale: 200 µm. (b) Relationship between fluorescence intensity changes of labeled brain tissue in response to electrical stimulation, by amperage of electrical pulse train. Linear trendline (dashed) is interpolated between data points ($R^2 = 0.9889$).

Sensor response was maintained after repeated cycles of stimulation and higher amperages (Fig. S5). This is consistent with Moreira et al., who studied the effect of Iowa Black RQ on DNA duplex stability, which ranked among the most stabilizing quenchers in a comparison study [33]. The intracellular nature of the K^+ Sensor is more relevant to both physiology and pathology, where the source of the K^+ fluctuations is the tissue itself [22]. Our K^+ Sensor showed a fractional fluorescence change of approximately 1% per 10 mA of applied stimulation current, which allows for the visualization of population-scale activity in live brain tissue.

4 Concluding Remarks

We have presented the design, synthesis, characterization, and biological applications of an aptamer-based potassium ion-sensing fluorescent nanoprobe. This nanosensor can monitor dynamic changes in intracellular K^+ levels upon external stimulation. These findings demonstrate that this nanoprobe may serve as a tool for real-time imaging of potassium ion-dependent processes in neural tissue. This is a first-generation probe for imaging of intracellular K^+ pools. However,

248 the limitation of ~1% fractional fluorescence change per 10 mA stimulation in tissue is notable
249 and will be a subject of improvement in future iterations of the probe design.

250 *4.1 Future Directions*

251 Future studies will focus on interchanging the selection of fluorophore and quencher pairs,
252 including those that emit in NIR wavelengths, and conjugating the platform with targeting ligands
253 for cell-specific binding. ICG dye is a candidate for conjugation to the aptamer sequence, given
254 that it emits in the NIR range and can penetrate living cells without inducing immediate
255 degenerative changes [34]. Ionic content in the intracellular space is known to cause dye
256 aggregation, quenching its fluorescence, although the effects of potassium have not been studied
257 specifically [35]. Conjugation to the oligonucleotide scaffold may help prevent dimerization, but
258 other techniques, such as lipid encapsulation, may also achieve this effect by shielding the dye
259 from the ionic aqueous environment [36]. With these improvements, sensor performance may be
260 evaluated in models of epileptic activity in tandem with EEG recordings. Future iterations of the
261 probe design will be used to monitor and record potassium ion dynamics during seizure-like
262 activity and in other model systems including cardiac models.

263 *Disclosures*

264 The authors declare that there are no financial interests, commercial affiliations, or other potential
265 conflicts of interest that could have influenced the objectivity of this research or the writing of this
266 paper.

267 *Animal Ethics Statement*

268 All animal procedures were approved by the Institutional Animal Care and Use Committee
269 (IACUC) at George Mason University (Protocol #0532) and conducted in accordance with the

National Institutes of Health Guide for the Care and Use of Laboratory Animals. Adult C57BL6/J mice (male and female, P30-90) were used for all experiments. Acute hippocampal brain slices were prepared as described in Section 2.4, and all efforts were made to minimize animal suffering and reduce the number of animals used.

Code, Data, and Materials

Data are available from the corresponding authors upon reasonable request.

Acknowledgments

This work was funded through the NSF award no. 2128821, NIH Project Number 1R01EB037718-01 and the Presidential Scholarship at George Mason University. The authors acknowledge the support of the IPN Microscopy Suite at George Mason University and the material contributions of the laboratory of Ted Dumas.

References

[1] J. Mitterdorfer and B. P. Bean, "Potassium Currents during the Action Potential of Hippocampal CA3 Neurons," *J Neurosci*, vol. 22, no. 23, pp. 10106–10115, Dec. 2002, doi: 10.1523/JNEUROSCI.22-23-10106.2002.

[2] A. L. Hodgkin and A. F. Huxley, "A quantitative description of membrane current and its application to conduction and excitation in nerve," *J Physiol*, vol. 117, no. 4, pp. 500–544, Aug. 1952.

[3] Andre. Haemmerli, Jiri. Janata, and H. Mack. Brown, "Ion-selective electrode for intracellular potassium measurements," *Anal. Chem.*, vol. 52, no. 8, pp. 1179–1182, Jul. 1980, doi: 10.1021/ac50058a006.

[4] J. R. Clay, "Axonal excitability revisited," *Progress in Biophysics and Molecular Biology*, vol. 88, no. 1, pp. 59–90, May 2005, doi: 10.1016/j.pbiomolbio.2003.12.004.

[5] C. R. Rose and A. Verkhratsky, "Principles of sodium homeostasis and sodium signalling in astroglia," *Glia*, vol. 64, no. 10, pp. 1611–1627, 2016, doi: 10.1002/glia.22964.

[6] J. Benedikt *et al.*, "Intracellular polyamines enhance astrocytic coupling," *NeuroReport*, vol. 23, no. 17, pp. 1021–1025, Dec. 2012, doi: 10.1097/WNR.0b013e32835aa04b.

[7] M. L. Olsen and H. Sontheimer, "Functional implications for Kir4.1 channels in glial biology: from K+ buffering to cell differentiation," *Journal of Neurochemistry*, vol. 107, no. 3, pp. 589–601, 2008, doi: 10.1111/j.1471-4159.2008.05615.x.

[8] A. Ortega, L. A. Martínez-Nuncio, E. Taddei, E. Castañeda, C. Rubio, and R.-O. Moisés, "ASTROGLIA: Molecular Mechanisms, Functional Roles, and Neurophysiological Implications in the Central Nervous System," *Life*, vol. 15, no. 10, pp. 1505–1526, 2025, doi: 10.3390/life15101505.

[9] M. Forsberg *et al.*, "Evaluation of mechanisms involved in regulation of intrinsic excitability by extracellular calcium in CA1 pyramidal neurons of rat," *Journal of Neurochemistry*, vol. 169, no. 1, p. e16209, 2025, doi: 10.1111/jnc.16209.

[10] B. P. Bean, "The action potential in mammalian central neurons," *Nat Rev Neurosci*, vol. 8, no. 6, pp. 451–465, Jun. 2007, doi: 10.1038/nrn2148.

[11] Y. Yaari, A. Konnerth, and U. Heinemann, "Nonsynaptic epileptogenesis in the mammalian hippocampus in vitro. II. Role of extracellular potassium," *Journal of Neurophysiology*, vol. 56, no. 2, pp. 424–438, Aug. 1986, doi: 10.1152/jn.1986.56.2.424.

[12] A. P. Fertziger and J. B. Ranck, "Potassium accumulation in interstitial space during epileptiform seizures," *Experimental Neurology*, vol. 26, no. 3, pp. 571–585, Mar. 1970, doi: 10.1016/0014-4886(70)90150-0.

[13] J. Sun, Y. Zheng, Z. Chen, and Y. Wang, "The role of Na^+ -K^+ - ATPASE in the epileptic brain," *CNS Neurosci Ther*, vol. 28, no. 9, pp. 1294–1302, Sep. 2022, doi: 10.1111/cns.13893.

[14] J. Zhang, X. Li, and J.-D. Li, "The Roles of Post-translational Modifications on α-Synuclein in the Pathogenesis of Parkinson's Diseases," *Front. Neurosci.*, vol. 13, 2019, doi: 10.3389/fnins.2019.00381.

[15] E. Samokhina, A. Mangat, C. S. Malladi, E. Gyengesi, J. W. Morley, and Y. Buskila, "Potassium homeostasis during disease progression of Alzheimer's Disease," May 23, 2024, *Neuroscience*. doi: 10.1101/2024.05.23.595252.

[16] V. M. Vitvitsky, S. K. Garg, R. F. Keep, R. L. Albin, and R. Banerjee, "Na+ and K+ ion imbalances in Alzheimer's disease," *Biochimica et Biophysica Acta (BBA) - Molecular Basis of Disease*, vol. 1822, no. 11, pp. 1671–1681, Nov. 2012, doi: 10.1016/j.bbadis.2012.07.004.

[17] M. Odijk *et al.*, "Microfabricated solid-state ion-selective electrode probe for measuring potassium in the living rodent brain: Compatibility with DC-EEG recordings to study spreading depression," *Sensors and Actuators B: Chemical*, vol. 207, pp. 945–953, Feb. 2015, doi: 10.1016/j.snb.2014.06.138.

[18] X. Tong *et al.*, "Astrocyte Kir4.1 ion channel deficits contribute to neuronal dysfunction in Huntington's disease model mice," *Nat Neurosci*, vol. 17, no. 5, pp. 694–703, May 2014, doi: 10.1038/nn.3691.

[19] J. Moon, Y. Ha, M. Kim, J. Sim, Y. Lee, and M. Suh, "Dual Electrochemical Microsensor for Real-Time Simultaneous Monitoring of Nitric Oxide and Potassium Ion Changes in a Rat Brain during Spontaneous Neocortical Epileptic Seizure," *Anal. Chem.*, vol. 88, no. 18, pp. 8942–8948, Sep. 2016, doi: 10.1021/acs.analchem.6b02396.

[20] Z. Zhu, J. Zhang, J. Zhu, W. Lu, and J. Zi, "Fabrication and Characterization of Potassium Ion-Selective Electrode Based on Porous Silicon," *IEEE Sensors J.*, vol. 7, no. 1, pp. 38–42, Jan. 2007, doi: 10.1109/JSEN.2006.888581.

[21] R. Ali, R. Almousa, S. M. Aly, and S. M. Saleh, "Nanoscale potassium sensing based on valinomycin-anchored fluorescent gold nanoclusters," *Mikrochim Acta*, vol. 191, no. 6, p. 299, May 2024, doi: 10.1007/s00604-024-06392-3.

[22] J. Wellbourne-Wood, T. S. Rimmele, and J.-Y. Chatton, “Imaging extracellular potassium dynamics in brain tissue using a potassium-sensitive nanosensor,” *Neurophoton*, vol. 4, no. 1, p. 015002, Feb. 2017, doi: 10.1117/1.NPh.4.1.015002.

[23] Y. Wang, Q. Wang, and X. Zhang, “A Novel Potassium Nanosensor Powers up the Detection of Extracellular K+ Dynamics in Neuroscience,” *Neurosci Bull*, vol. 36, no. 12, pp. 1573–1575, Sep. 2020, doi: 10.1007/s12264-020-00572-w.

[24] Z. Wang, T. C. Detomasi, and C. J. Chang, “A dual-fluorophore sensor approach for ratiometric fluorescence imaging of potassium in living cells,” *Chem. Sci.*, vol. 12, no. 5, pp. 1720–1729, 2021, doi: 10.1039/D0SC03844J.

[25] M. Massey, W. R. Algar, and U. J. Krull, “Fluorescence resonance energy transfer (FRET) for DNA biosensors: FRET pairs and Förster distances for various dye–DNA conjugates,” *Analytica Chimica Acta*, vol. 568, no. 1–2, pp. 181–189, May 2006, doi: 10.1016/j.aca.2005.12.050.

[26] D. Bhattacharyya, G. Mirihana Arachchilage, and S. Basu, “Metal Cations in G-Quadruplex Folding and Stability,” *Front. Chem.*, vol. 4, Sep. 2016, doi: 10.3389/fchem.2016.00038.

[27] Y. Yang *et al.*, “Aptamer-based FRET nanoflares for imaging potassium ions in living cells,” *Chem. Commun.*, vol. 52, no. 76, pp. 11386–11389, Sep. 2016, doi: 10.1039/C6CC05379C.

[28] S. O. Thier, “Potassium physiology,” *The American Journal of Medicine*, vol. 80, no. 4, Supplement 1, pp. 3–7, Apr. 1986, doi: 10.1016/0002-9343(86)90334-7.

[29] J. C. Octeau, G. Faas, I. Mody, and B. S. Khakh, “Making, Testing, and Using Potassium Ion Selective Microelectrodes in Tissue Slices of Adult Brain,” *JoVE*, no. 135, p. 57511, May 2018, doi: 10.3791/57511.

[30] B. J. Müller *et al.*, “Nanoparticle-Based Fluoroionophore for Analysis of Potassium Ion Dynamics in 3D Tissue Models and In Vivo,” *Advanced Functional Materials*, vol. 28, no. 9, p. 1704598, 2018, doi: 10.1002/adfm.201704598.

[31] D. A. Coulter *et al.*, “Hippocampal microcircuit dynamics probed using optical imaging approaches,” *The Journal of Physiology*, vol. 589, no. 8, pp. 1893–1903, 2011, doi: 10.1113/jphysiol.2010.202184.

[32] M. H. Mohajerani, S. Sivakumaran, P. Zacchi, P. Aguilera, and E. Cherubini, “Correlated Network Activity Enhances Synaptic Efficacy via BDNF and the ERK Pathway at Immature CA3-CA1 Connections in the Hippocampus,” *Proceedings of the National Academy of Sciences of the United States of America*, vol. 104, no. 32, pp. 13176–13181, 2007.

[33] B. G. Moreira, Y. You, M. A. Behlke, and R. Owczarzy, “Effects of fluorescent dyes, quenchers, and dangling ends on DNA duplex stability,” *Biochemical and Biophysical Research Communications*, vol. 327, no. 2, pp. 473–484, Feb. 2005, doi: 10.1016/j.bbrc.2004.12.035.

[34] J. S. Díaz Tovar, G. Kassab, N. M. Inada, V. S. Bagnato, and C. Kurachi, “Photobleaching Kinetics and Effect of Solvent in the Photophysical Properties of Indocyanine Green for Photodynamic Therapy,” *ChemPhysChem*, vol. 24, no. 18, p. e202300381, Sep. 2023, doi: 10.1002/cphc.202300381.

[35] B. Chon, W. Ghann, J. Uddin, B. Anvari, and V. Kundra, “Indocyanine Green (ICG) Fluorescence Is Dependent on Monomer with Planar and Twisted Structures and Inhibited by H-Aggregation,” *Int J Mol Sci*, vol. 24, no. 17, p. 13030, Aug. 2023, doi: 10.3390/ijms241713030.

[36] A.-K. Kirchherr, A. Briel, and K. Mäder, “Stabilization of Indocyanine Green by Encapsulation within Micellar Systems,” *Mol. Pharmaceutics*, vol. 6, no. 2, pp. 480–491, Apr. 2009, doi: 10.1021/mp8001649.